photonics

MDPI

Article

Erbium-Doped Fiber Laser Q-Switched and Mode-Locked by Red-Fluorescent Carbon-Quantum-Dot-Based Saturable Absorber

Tian-Run Liu [1], Xue-Peng Zhu [1], Jiong Liu [2], Zi-Qi Zhang [1], Wen-Fei Zhang [2,*], Wen-Jing Tang [3] and Xiao-Juan Liu [1,*]

[1] School of Physics and Optoelectronic Engineering, Shandong University of Technology, Zibo 255049, China; 24512021162@stumail.sdut.edu.cn (T.-R.L.); 25512021196@stumail.sdut.edu.cn (X.-P.Z.); zhangzq@sdut.edu.cn (Z.-Q.Z.)
[2] College of Physics and Optoelectronic Engineering, Shenzhen University, Shenzhen 518060, China; 2300453046@email.szu.edu.cn
[3] School of Physics and Technology, University of Jinan, Jinan 250022, China; sps_tangwj@ujn.edu.cn
* Correspondence: zhangwf@szu.edu.cn (W.-F.Z.); liuxiaojuan@sdut.edu.cn (X.-J.L.)

Abstract

A pulsed erbium-doped fiber laser (EDFL) incorporating a saturable absorber (SA) based on red-fluorescent carbon quantum dots (RCQDs) is experimentally demonstrated. First, an RCQD-based, fiber-compatible sandwich-structured SA is fabricated and the nonlinear saturable absorption property (NSAP) is characterized. When the as-prepared RCQDs-SA is integrated into the EDFL with a ring cavity construction, Q-switching and conventional-soliton (CS) mode-locking operations of the laser system are achieved. Stable Q-switching and mode-locking are achieved over pump power ranges of 310–520 mW and 450–590 mW, respectively. In the pump power range of 450–520 mW, the EDFL is robust for switching between Q-switching and mode-locking regimes. The RCQDs-SA exhibits a modulation depth of 11.84% and enables passive Q-switching and passive CS mode-locking when integrated into the EDFL ring cavity. This work, together with our previous ultrafast EDFL mode-locked by green-fluorescent carbon quantum dots (GCQDs) SA, lays a solid foundation for the application and development of carbon quantum dots (CQDs) in the field of ultrafast lasers.

Keywords: red-fluorescent carbon quantum dots; saturable absorber; Q-switching; mode-locking; erbium-doped fiber laser

1. Introduction

Q-switching and mode-locking are two widely used approaches to generating pulses in fiber lasers. Both regimes can be realized through active or passive modulation, and switching between them has been demonstrated in a fiber laser incorporating a large-angle tilted fiber grating [1]. Passive modulation is attractive in practice because it avoids the need for an external modulator. For example, passive Q-switching has been achieved with saturable absorbers based on graphene, transition-metal chalcogenides, and zirconia nanoparticles [2–7]. Among carbon nanomaterials, carbon nanotubes (CNTs) have been widely studied as saturable absorbers for ultrashort pulse generation in passively mode-locked fiber lasers [8].

CQDs are another class of carbon nanomaterials, with typical particle sizes ranging from 1 to 10 nm [9]. Due to the characteristics of stability and universality, CQDs achieve

Check for updates

Received: 1 November 2026
Revised: 18 November 2026
Accepted: 24 November 2026
Published: 27 November 2026

Copyright: © 2026 by the authors. Licensee MDPI, Basel, Switzerland. This article is an open access article distributed under the terms and conditions of the Creative Commons Attribution (CC BY) license.

"one material for multiple purposes and cross-field integration" [10,11]. CQDs can be considered admirable materials for multifunctional, low-cost, and bio-friendly photonic devices [12–17]. The optical and electronic properties of CQDs make them promising for optoelectronic applications [18–23]. CQDs can exhibit broad excitation and narrow emission bands and offer advantages such as low toxicity, high stability, and low cost [9–15]. In addition, CQDs have high chemical stability [11–16] and good photobleaching resistance [10–16]. Furthermore, CQDs are free from heavy metal pollution; hence, they present excellent biocompatibility [11,13]. Based on the characteristics listed above, CQDs are found to be an admirable candidate for solving the troubles faced by traditional nanomaterials in terms of safety and stability, and have shown outstanding research and application value in fields such as bioimaging, sensing detection, environmental remediation, photocatalysis, and electrocatalysis [14,15].

Different from existing CQD research, our research group focuses on the NSAP of CQDs and the regimes of pulse output of fiber lasers modulated by CQD-based optical devices. In 2024, our group explored CS mode-locking, fundamental mode-locking, and 20th harmonic mode-locking of an EDFL based on the NSAP of GCQDs [17]. Our group has also demonstrated passive mode-locking in EDFLs using InSb, $TiSe_2$, and InSe as saturable absorbers [24–26]. Here, we demonstrate switchable operation between passive Q-switching and passive conventional soliton mode-locking in a single erbium-doped fiber ring cavity using a sandwich-structured saturable absorber based on RCQDs. At the beginning, the RCQDs are synthesized using a solvothermal method. After a series of characterizations, the as-prepared RCQDs are fabricated into a sandwich-structured RCQDs-SA device. Then, the NSAP of the RCQDs-SA device is tested and confirmed. In the Q-switched regime, the pulse width is compressed from 8.7 μs to 4.55 μs, while the pulse repetition rate is simultaneously increased from 17.94 kHz to 34.36 kHz. The available maximum average output power is 0.31 mW. When the pump power is increased to 450 mW, the system can be switched into a CS mode-locked regime by modulating the inner-cavity polarization controller (PC). Mode-locking remains stable in the pump power range of 450–590 mW. The pulse duration of the laser is 871 fs. These results demonstrate that the fiber-compatible RCQDs-SA can be used for passive pulse generation in an erbium-doped fiber laser.

2. Materials and Methods

2.1. Synthesis and Characterization of RCQDs Sample

The solvothermal method is commonly employed for the synthesis of quantum dot nanomaterials. In our experiment, 10 mg of naphthalenediamine, 10 mL of anhydrous ethanol, and 3 mL of concentrated H_2SO_4 are charged into a polytetrafluoroethylene(PTFE)-lined autoclave reactor. Then, the mixture undergoes ultrasonication for 10 min and is immediately transferred into a drying oven and reacts at 190 °C for 3 h. After natural cooling, an unpurified RCQDs solution with a dark green color is obtained. In the as-prepared solution, the contents, in descending order, are yellow, red, and deep-red CQDs, respectively. In order to obtain pure RCQDs, using a mixture of methanol and dichloromethane at a volume ratio of 7:50 as the eluent, the solution is subjected to silica column chromatography. Consequently, the RCQD solution is successfully obtained, which presents a clear red color, as shown in Figure 1.

Subsequently, a series of characterizations are conducted. First, X-ray diffraction (XRD) measurements are performed on an X-ray diffractometer(Rigaku SmartLab (Rigaku, Tokyo, Japan)). As shown in Figure 2a, a distinct diffraction peak is observed at $2\theta = 25°$, which verifies that the present sample is purified RCQDs. Then, the surface morphology and particle size of the RCQDs are examined using a transmission electron microscope(TEM)(JEOL JEM-2100(JEOL, Tokyo, Japan)) As presented in Figure 2b, the RCQDs exhibit a nearly

uniform spherical morphology. In addition, the RCQDs disperse homogeneously in the suspension and no aggregation of the quantum dots is observed. The statistical TEM analysis of RCQDs is shown in Figure 2c. It is seen that the diameter of RCQDs ranges from 2 to 5 nm, with the statistical average particle diameter of 3.2 nm. The measured diameter values fall within the typical size range of CQDs (1–10 nm).

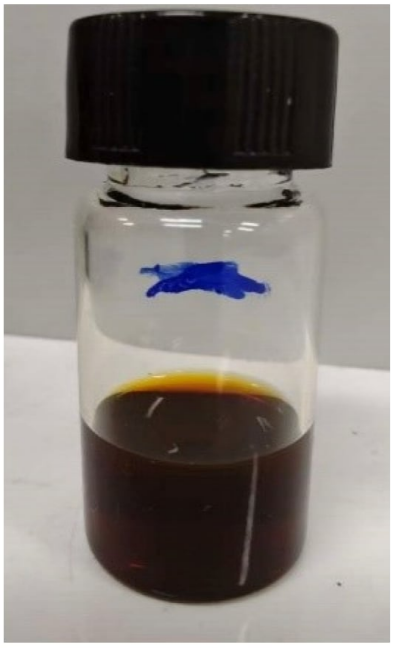

Figure 1. Dichloromethane solution of RCQDs.

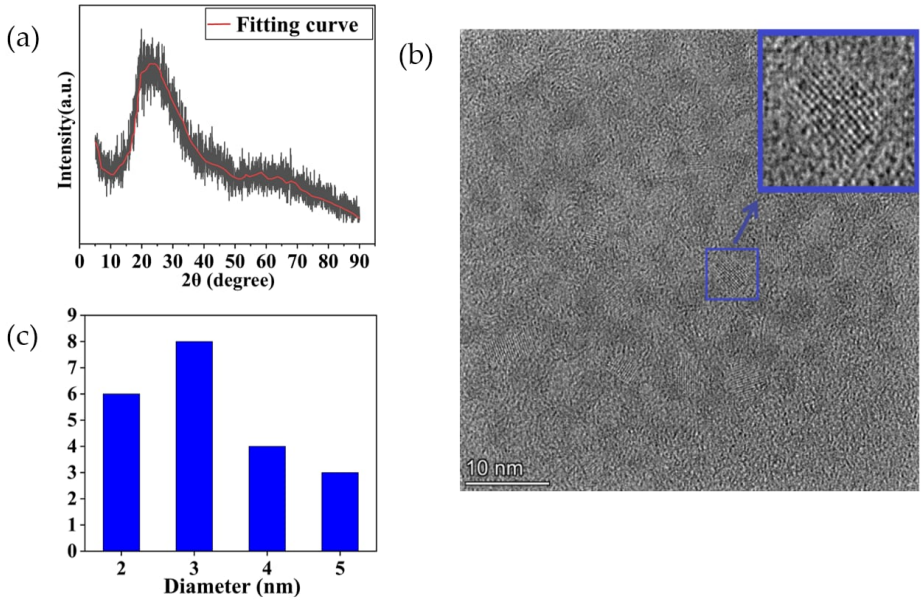

Figure 2. RCQDs characterization. (**a**) XRD pattern. (**b**) TEM image. (**c**) Particle size statistics.

To further study the characteristics of the as-prepared RCQDs, the absorption and fluorescence spectra of the RCQDs are measured using an FS5 spectrometer (Edinburgh Instruments, UK), which are shown in Figure 3a,b. It's known that RCQDs can emit red fluorescence under laser radiation in the green light band. So, in order to visually verify the absorption and fluorescence spectrum characteristics, we irradiate the RCQDs solution with a laser emitting light around 540 nm. As presented in Figure 3c, the RCQDs solution

emits bright and red fluorescence visible to the naked eye. All of the above confirms the authenticity of the RCQDs.

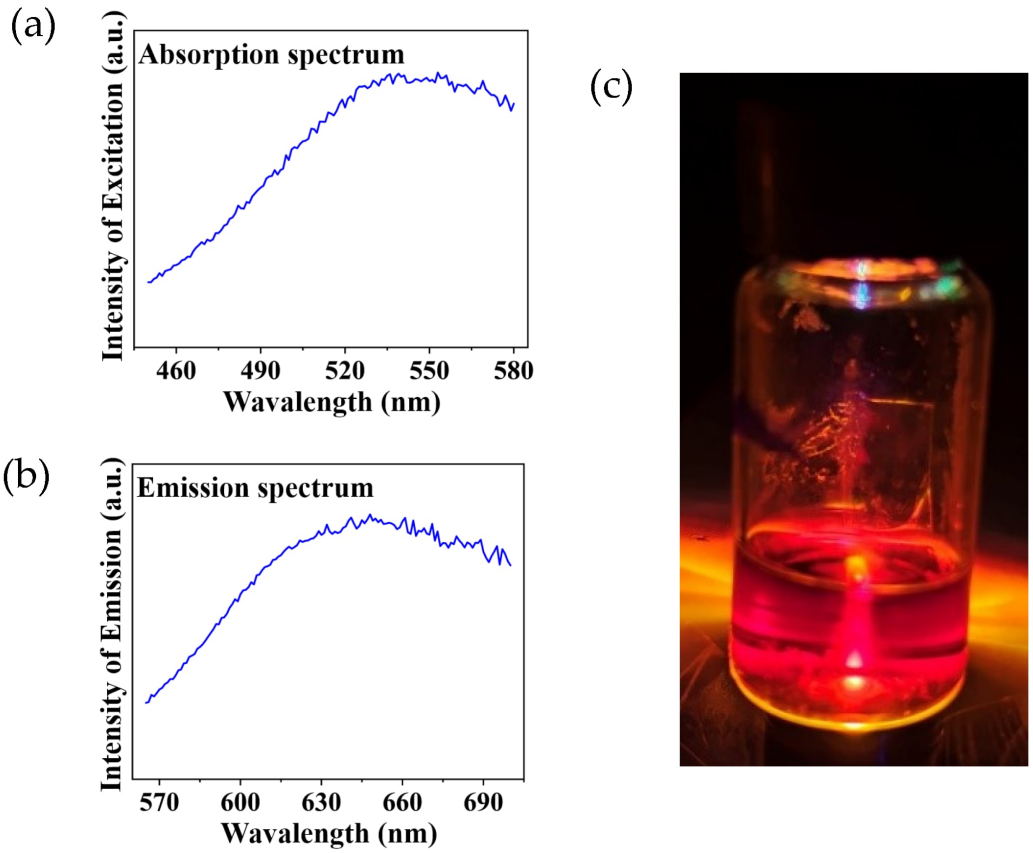

Figure 3. (**a**) Absorption spectrum. (**b**) Emission spectrum. (**c**) Photograph of RCQDs solution under irradiation.

2.2. Fabrication and Characterization of RCQDs-SA

To facilitate integration and use, a fiber-compatible sandwich-structured RCQDs-SA is fabricated. In this work, the RCQDs solution is first mixed with a 4 wt% PVA aqueous solution at a volume ratio of 1:1.5. The mixture is then subjected to ultrasonication for 4 h to yield a homogeneous RCQDs-PVA dispersion. Subsequently, the resulting dispersion is spin-coated onto the bottom of a Petri dish. After drying naturally in ambient air at room temperature, RCQDs-PVA films are synthesized. Finally, the RCQDs-PVA films are cut into small pieces, and with one piece of RCQDs-PVA film sandwiched between two fiber connector end faces and assembled via flange connection, a transmissive sandwich-structured RCQDs-SA is ultimately fabricated.

In order to improve the energy conversion efficiency of the fiber laser systems, each optical component in the fiber cavity should have as little insertion loss (IL) as possible. Considering that the prepared RCQDs-SA device belongs to a new passive optical device, its IL is measured as presented in Figure 4a. The light source is composed of a laser diode (LD) with a central wavelength of 976 nm and an erbium-doped fiber (EDF, Er-110-4/125) with a length of 0.3 m. In addition, a 980/1550 nm wavelength division multiplexer (WDM) is adopted to couple the LD pump light into the EDF to generate an amplified spontaneous emission (ASE) spectrum. A coaxial polarization-independent isolator (PI-ISO) is used to ensure the unidirectional propagation of the signal light. The output powers with and without the RCQDs-SA device inserted into the light path are measured and recorded as Po and Pi, respectively. Then, the transmittance of the RCQDs-SA device is defined as

T = Po/Pi, and the T data versus pump powers are shown in Figure 4b. As a result, the average value of T is calculated to be 0.764, from which the IL is determined to be 1.167 dB.

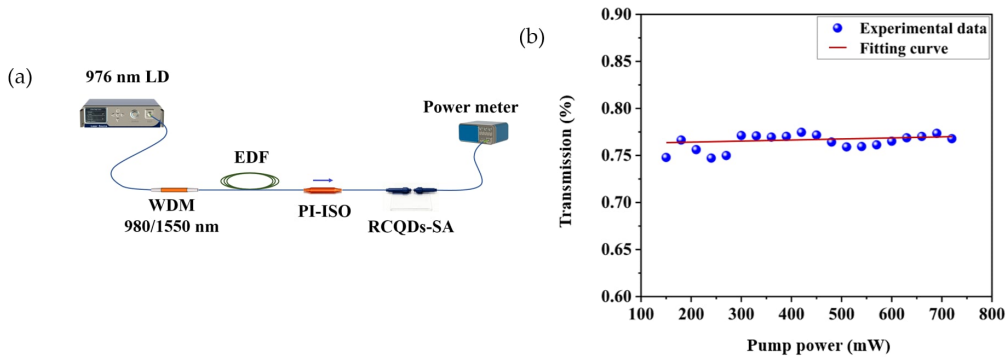

Figure 4. (**a**) Experimental diagram for IL test of the sandwich-structured RCQDs-SA. (**b**) The transmittance of the RCQDs-SA.

Effective modulation and pulse generation in the fiber laser depend on the nonlinear saturable absorption of the as-prepared RCQDs-SA. To characterize this response, we used the same balanced twin-detector measurement setup as that described in Ref. [17]. In the arrangement shown in Figure 5a, the laser source delivered 300 fs pulses at a wavelength of 1560 nm and a repetition rate of 80 MHz. The laser beam is equally split into two paths by a 50:50 fiber-optic coupler (50:50 OC). One path, serving as reference light, is detected by Power Meter 1. The other path, serving as signal light, is detected by Power Meter 2 after transmitting through the RCQDs-SA device. The intensity is adjusted by an attenuator. The blue dots in Figure 5b represent the apparent absorption inferred from the transmission measurements, calculated as

$$100(1 - T), \tag{1}$$

where T is the transmittance of the RCQDs-SA, and the red line shows the fit.The fitting was performed with OriginPro 2021 (OriginLab Corporation, Northampton, MA, USA). As the incident peak intensity increases, the saturable component of the absorption decreases, and the curve approaches a plateau. The measurements in Figure 5b show that the absorption of the RCQDs-SA varies with incident peak intensity. The red curve represents the fit to these data. The fit yielded a modulation depth of 11.84% and a saturation intensity of 5.88 MW/cm^2, which characterize the nonlinear saturable absorption properties of the RCQDs-SA.

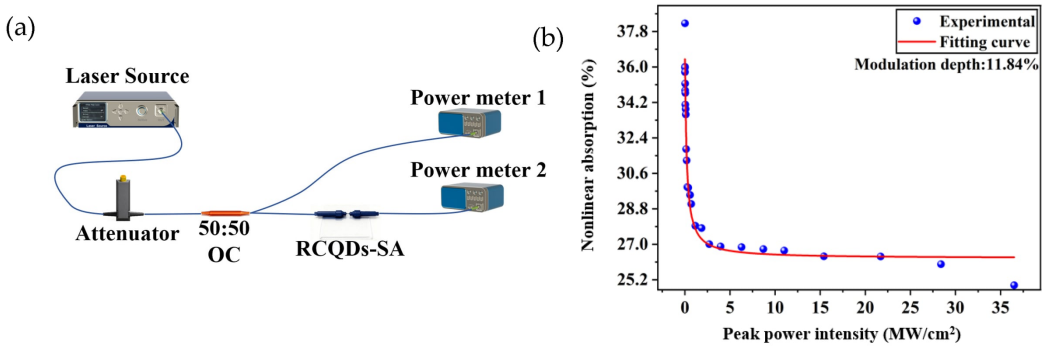

Figure 5. (**a**) Layout of the balanced twin-detector setup. (**b**) Nonlinear absorption of the RCQDs-SA as a function of incident peak intensity.

2.3. Experimental Setup

To investigate the modulation capability of the RCQDs, as shown in Figure 6, an EDFL system is proposed and constructed with a classic ring cavity. First of all, the four optical instruments and devices, including LD, WDM, EDF and PI-ISO, are the same as those in Figure 4a. The other components involved in the EDFL system include an OC, a paddle-type PC, the prepared RCQDs-SA and a 17 m single-mode fiber (SMF-28). Among them, the PC is utilized to optimize the polarization state of the whole fiber cavity. The function of the OC is to extract a provision of 10% of the intra-cavity laser for analysis, including, but not limited to, spectral monitoring [Optical Spectrum Analyzer, YOKOGAWA AQ6370B (Tokyo, Japan)], radio-frequency observation [Radio Frequency Spectrum Analyzer, FPC1000 (Rohde & Schwarz, Munich, Germany)], pulse duration test [Autocorrelator, Femtochrome FR-103XL (Berkeley, CA, USA)], and output power measurement [Power Meter, PM3 (Molotron, Portland, OR, USA)]. The overall cavity length, including the EDF, SMF-28 and all involved fiber pigtails, is 19 m. The calculated net cavity dispersion was -0.382 ps^2, based on chromatic dispersion coefficients of 17.0 ps/(nm·km) for the SMF-28 fiber and 7.5 ps/(nm·km) for the EDF.

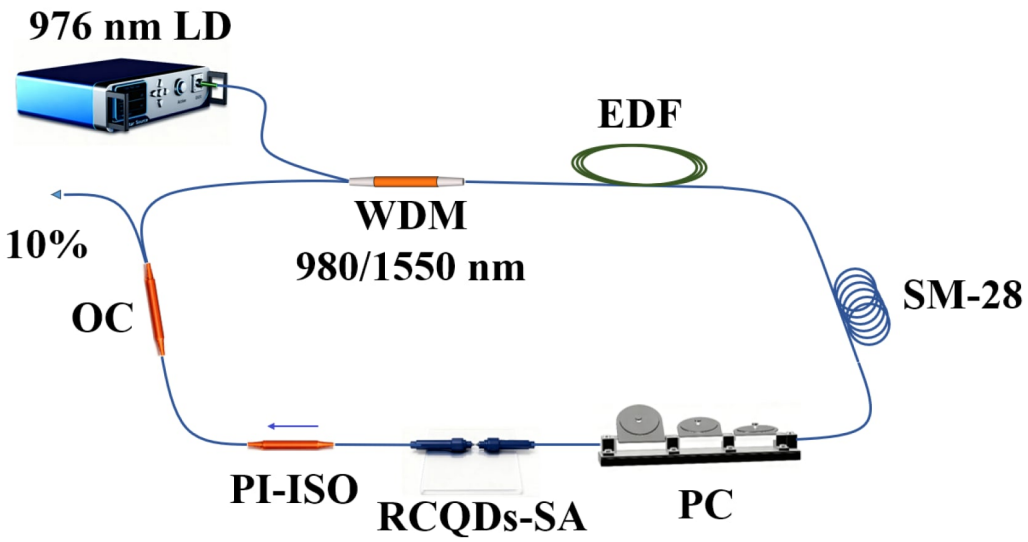

Figure 6. Schematic of the ring cavity. The arrow indicates the direction of light propagation inside the cavity.

3. Results and Discussion

3.1. Q-Switched

The EDFL emitted only continuous-wave (CW) light when the RCQDs-SA was absent, across the full range of accessible LD pump powers and PC settings. After the absorber was installed in the cavity, Q-switching was the first stable pulsed regime observed and was sustained over a pump power range of 310–520 mW. The pulse trains in Figure 7 show an increase in repetition rate with pump power, a characteristic trend of Q-switched operation.

Figure 8a quantifies this trend. Increasing the pump power from 310 to 520 mW shortened the pulses from 8.7 to 4.55 μs and raised the repetition rate from 17.94 to 34.36 kHz. The average output power and single-pulse energy both increased monotonically over the same range (Figure 8b), reaching their respective maxima of 0.31 mW and 9.1 nJ at 520 mW.

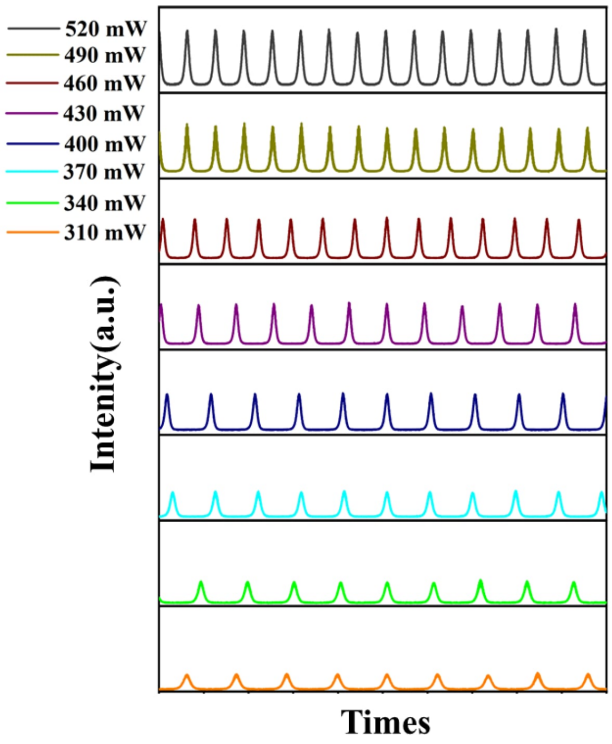

Figure 7. Q-switched pulse sequences under different pump powers.

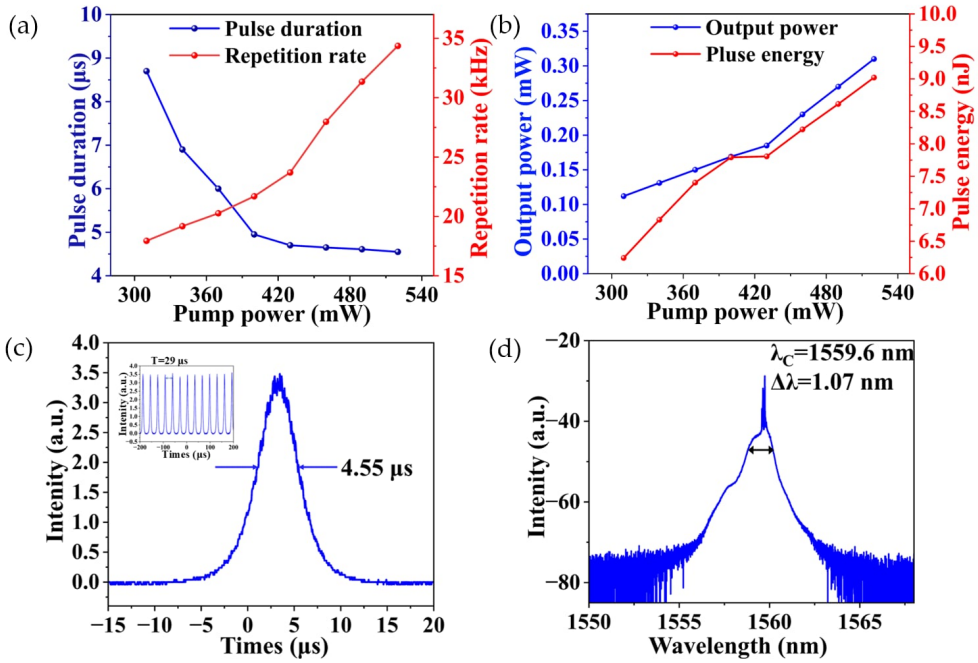

Figure 8. Q-switching performance of the EDFL. (**a**) Pulse repetition rate and duration versus pump power. (**b**) Average output power and pulse energy versus pump power. (**c**) Q-switched pulse envelope recorded at a pump power of 520 mW. (**d**) Optical spectrum of the Q-switched output.

At the pump power upper limit for the stable Q-switched regime, the pulse envelope is the narrowest, as depicted in Figure 8c. The inset presents the oscilloscope traces of the Q-switched pulse sequence with a pulse interval of 29 μs, exhibiting excellent stability without obvious fluctuations on the oscilloscope. According to Formula (2),

$$f = 1/T \quad (2)$$

where f is the repetition rate and T is the pulse interval, respectively, and the repetition rate is theoretically calculated to be 34.36 kHz, which is consistent with the experimental result. As illustrated in Figure 8d, the optical spectrum locates at the central wavelength of 1559.6 nm and possesses a 3 dB bandwidth of 1.07 nm.

For practical applications of Q-switched lasers in various fields, parameters such as pulse duration, pulse energy, and output average power are crucial. In order to comprehensively evaluate the Q-switched pulses obtained in this experiment, a comparison of the core parameters among various EDFLs modulated by different kinds of SAs is summarized and listed in Table 1.

Table 1. Comparison of passively Q-switched EDFLs based on different SAs.

Materials	Threshold Pump Power (mW)	Central Wavelength (nm)	Pulse Duration (μs)	Pulse Energy (nJ)	Max Output Power (mW)	Ref.
Graphene	6.5	1556.17	3.7	16.7	1.1	[5]
ZrO_2	19.36	1558.66	7.90	9	1.17	[6]
MoTe2	225	1559	0.677	109	25	[7]
TiCN	330	2778	5.4	-	25.83	[27]
Fe_3O_4	50	1566.9	5.7	126	6.51	[28]
SWNT	800	1530.4	2.19	58.37	12.3	[29]
TiO_2	50	1534	0.08	-	0.075	[30]
CNTs	50	1498.3	3.4	7.6	0.5	[31]
$ZrGeTe_4$	55	1560	1.24	57.36	3.88	[32]
RCQDs	310	1559.6	4.55	9.1	0.31	Our work

As shown in Table 1, at a similar central wavelength, the RCQDs-based laser produces shorter Q-switched pulses than the ZrO_2-based laser reported in Ref. [6] (4.55 μs versus 7.90 μs), with comparable pulse energies (9.1 nJ versus 9.0 nJ). The pulse duration is also shorter than the 5.7 μs reported for the Fe_3O_4-based laser [28], which delivers a higher pulse energy of 126 nJ.

3.2. Conventional-Soliton Mode-Locking

According to the theoretical reports [1–4], short cavities typically facilitate the Q-switched regime in fiber lasers, while long cavities promote the accumulation of nonlinear effects, thereby favoring the mode-locked regime. Our previous works, including the Q-switched [2–4] and mode-locked [24–26] EDFLs, consistently align with this principle. In this experiment, the length of the laser ring cavity is initially set to 19 m and the cavity net dispersion is calculated to be -0.382 ps^2, so mode-locking is expected in this configuration, and the Q-switched regime is first achieved, which is a surprise and strongly proves the efficient saturable absorption effect of the RCQDs-SA device. The reason why the pump threshold is relatively high is first attributed to the high saturation intensity of the RCQDs-SA device [5]. Second, the long cavity increases the transmission loss of the optical circuit and as a result, the pump threshold for Q-switching is raised. So, it is rational to believe that the pump threshold can be dropped and the output power can be further scaled up by optimizing the cavity configuration for Q-switched operation.

At lower pump powers, the balance between gain and loss in a fiber laser cavity can favor Q-switching, producing pulses with durations in the nanosecond or microsecond range. As the pump power increases, nonlinear effects can become more pronounced, and their interplay with cavity dispersion can favor the formation of picosecond or femtosecond pulses in the mode-locked regime. Both Q-switched and mode-locked operation have been reported in a thulium-doped fiber laser using water as a saturable absorber [33]. In our

EDFL, increasing the pump power and fine-tuning the PC paddles led to CS mode-locking, consistent with the net anomalous dispersion of the cavity. This regime remained stable over a pump power range of 450–590 mW.

First, the output spectrum with a central wavelength and a 3 dB bandwidth of 1560.50 nm and 3.40 nm is shown in Figure 9a. Several pairs of Kelly sidebands are symmetrically distributed with respect to the central wavelength, revealing the typical CS mode-locking characteristics of the present operation. Second, the pulse sequence in Figure 9b presents a pulse interval of 91 ns. According to the Formula (1), the repetition rate is theoretically calculated to be 10.99 MHz. Then, the RF spectrum and the signal-to-noise ratio (SNR) are measured and depicted in Figure 9c. The repetition rate is experimentally tested to be 10.97 MHz, which is in accordance with the cavity length and the calculation. The SNR value is tested to be 52.51 dB, which, combining the clean RF spectrum within a 200 MHz span shown as an inset, verifies the high stability of the mode-locking operation. As illustrated in Figure 9d, the pulse duration is measured to be 871 fs, which corresponds to a time-bandwidth product (TBP) of 0.365 and indicates that the pulse is weakly chirped.

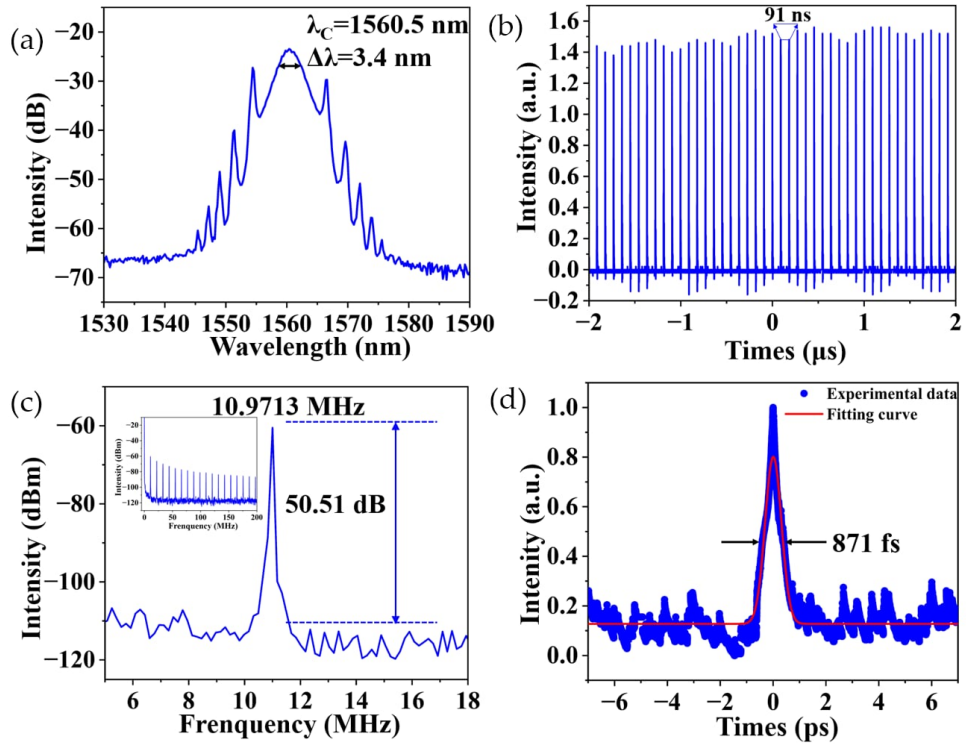

Figure 9. Characterization of conventional soliton mode-locking in the erbium-doped fiber laser. (**a**) Optical spectrum showing Kelly sidebands. (**b**) Pulse train with a 91 ns spacing between consecutive pulses. (**c**) Radio-frequency spectrum, with a 200 MHz span shown in the inset. (**d**) Autocorrelation trace yielding a pulse duration of 871 fs.

As shown in Figure 10, both the average output power and the output pulse energy increase approximately linearly as the pump power rises from 450 to 590 mW. No clear roll-off in the average output power is observed over this range. At a pump power of 590 mW, the average power measured at the 10% port of the output coupler reaches 0.55 mW. According to Formula (3),

$$E_p = P_{avg}/f_r \tag{3}$$

where P_{avg} is the average output power measured at the 10% output port, f_r is the repetition rate, and the pulse energy E_p is determined to be 0.05 nJ.

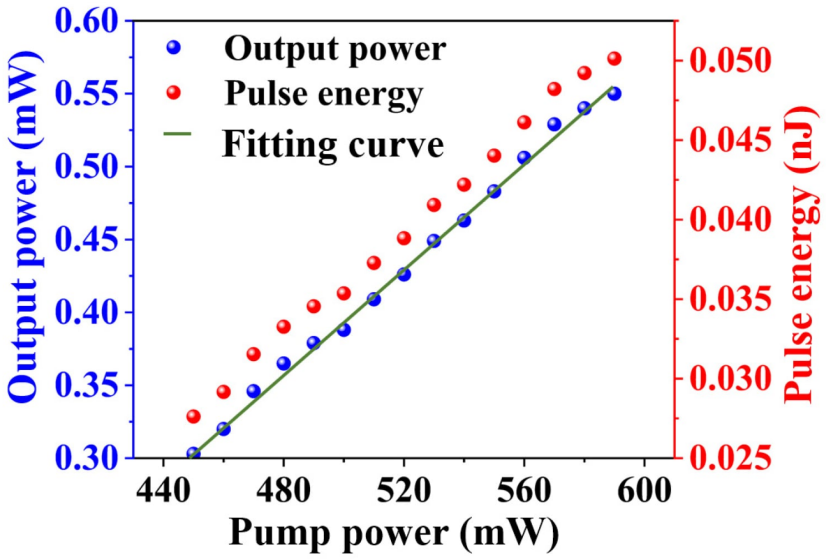

Figure 10. Output power and pulse energy versus pump power.

It is widely accepted that the modulation depth falling within the range of 5–20% is an admirable condition for a high-performance SA [2–4,34,35]. Considering that the modulation depth of the RCQDs-SA in this work is 11.84%, excellent modulation results are expected. As shown in Table 2, the mode-locked pulse duration of 871 fs is shorter than the 1260 fs reported for the $ZrGeTe_4$-based laser [34] and longer than the 675 fs reported for the WS_2-based laser [36]. Differences in laser cavity configurations and operating conditions across studies limit direct comparisons of the performance metrics listed in Tables 1 and 2.

Table 2. Comparison of mode-locked EDF lasers based on different real SAs.

Materials	Modulation Depth (%)	Central Wavelength (nm)	Repetition Rate (MHz)	Pulse Duration (fs)	SNR (dB)	Output Power (mW)	Ref.
Ge8Sb92	16.58	1879.88	20.04	1005	92	16.6	[37]
PbS	43.87	1569	9.18	550	50	19.5	[38]
WS2	1.2	1558.5	19.58	675	67	0.625	[36]
PbS/CdS	4.95	1562.5	3.30	54,000	>50	2.71	[39]
CQDs	18.9	1561.5	23.8	675	74.78	4.26	[17]
Sb2Te3	3.9	1556	22.13	449	74	0.9	[40]
Bi2Se3	3.9	1557.5	12.5	660	>55	1.8	[41]
CuO	6.82	1530.2	5.34	1230	53	2.2	[42]
$ZrGeTe_4$	14.5	1561.10	4.38	1260	59	0.35	[34]
RCQDs	11.84	1560.5	10.97	871	52.51	0.55	Our work

4. Discussion

Within the overlapping pump power range of 450–520 mW, the laser could be switched between passive Q-switching and conventional soliton mode-locking by adjusting the intracavity PC at a fixed pump power. Rotating the PC paddles changes the orientation of the birefringent fiber loops and thereby adjusts the intracavity polarization state. During PC adjustment, the output pulse train can be monitored on an oscilloscope. The Q-switched pulse train has a repetition rate in the kilohertz range, whereas the mode-locked pulse train has a repetition rate in the megahertz range, with a pulse spacing of approximately 91 ns. To reproduce the transition, the pump power can be held fixed within the overlapping range while the PC paddles are adjusted from a stable Q-switched state. The oscilloscope trace

provides feedback for locating a PC setting that yields a stable megahertz-rate pulse train. The RF peak at 10.97 MHz, corresponding to the cavity round-trip frequency, and the Kelly sidebands in the optical spectrum can then be used to verify fundamental conventional soliton mode-locking.

As described in Section 3.1, after the RCQDs-SA was removed, only continuous-wave operation was observed over the tested ranges of pump power and PC settings. This control indicates that the RCQDs-SA was required for pulsed operation under the conditions tested. The dependence of the operating regime on the PC setting also shows that the intracavity polarization state influences regime selection. Although the cavity in Figure 6 uses a polarization-independent isolator, any residual polarization-dependent loss in the cavity could convert nonlinear polarization evolution (NPE) into intensity-dependent transmission. NPE could therefore act together with the RCQDs-SA, particularly during mode-locking.

RCQDs investigated in this work and the GCQDs reported in our previous study [17] were both prepared by solvothermal synthesis. Naphthalenediamine was used as the precursor for the RCQDs, while citric acid and hexamethylenetetramine were used for the GCQDs. Precursor chemistry can influence the formation of π-conjugated carbon domains and the composition of surface functional groups, thereby modifying the electronic states involved in emission. The RCQDs emit at a longer wavelength than the GCQDs, corresponding to a lower-energy radiative transition. This difference in radiative transition energy is the fundamental distinction between the emission properties of the two materials. Differences in the distribution of electronic states may also affect the optical transitions near 1.55 μm and the dependence of absorption on incident intensity. The two sandwich-structured saturable absorbers exhibited similar modulation depths of 11.84% for the RCQDs-SA and 12.0% for the GCQDs-SA [17]. The RCQDs-SA had a saturation intensity of 5.88 MW/cm^2, approximately 36% lower than the value of 9.16 MW/cm^2 reported for the GCQDs-SA [17]. According to the saturation model used, the RCQDs-SA therefore requires a lower incident peak intensity to achieve the same fractional reduction in saturable absorption under the reported measurement conditions. The two types of carbon quantum dots were synthesized from different precursors, and the laser experiments used different cavity configurations. The earlier GCQDs-based laser exhibited several mode-locking regimes within a single cavity [17]. By combining an RCQDs-based absorber synthesized from a different precursor with a different cavity configuration, the present study extends our earlier work on GCQDs-based mode-locking by demonstrating switchable operation between passive Q-switching and passive conventional soliton mode-locking within a single fiber cavity.

The RCQDs-SA was fabricated using a 4 wt% PVA solution. All experiments reported in this study were completed within a one-year period. During this period, the RCQDs-SA repeatedly supported stable Q-switched and mode-locked operation, with stable average output power during measurements in both regimes. The highest measured average output powers were 0.31 mW for Q-switching and 0.55 mW for mode-locking. These observations demonstrate that the RCQDs-SA remained functional over the course of the experimental campaign. The PVA matrix served as the host for the RCQDs in the absorber film. The stable pulsed operation and output power observed in repeated measurements indicate that the RCQDs–PVA film retained sufficient functional stability throughout the one-year experimental period under the conditions tested.

5. Conclusions

We experimentally demonstrate a compact erbium-doped fiber laser incorporating an RCQDs-based saturable absorber. Within the pump power ranges of 310–520 mW and 450–590 mW, stable Q-switching and mode-locking are readily achieved. A single RCQDs-

SA enables both passive Q-switching and passive conventional soliton mode-locking in the same erbium-doped fiber ring cavity, with minimum pulse durations of 4.55 μs and 871 fs, respectively. Within the pump power range of 450–520 mW, the laser can be switched between the two regimes by adjusting only the intracavity PC. These results demonstrate the feasibility of using red-fluorescent carbon quantum dots as the saturable absorber material in pulsed fiber lasers. The ability to switch between passive Q-switching and conventional soliton mode-locking in a single fiber cavity provides an experimental basis for exploring how cavity design and absorber properties can be optimized to broaden the pump power range over which the two regimes can be switched.

Author Contributions: Conceptualization, X.-J.L.; Investigation, T.-R.L., X.-P.Z., Z.-Q.Z. and W.-F.Z.; Resources, J.L. and W.-F.Z.; Data Curation, T.-R.L. and Z.-Q.Z.; Writing—Original Draft, T.-R.L.; Writing—Review and Editing, X.-J.L. Validation, T.-R.L. and X.-P.Z.; Supervision, W.-J.T. and X.-J.L. All authors have read and agreed to the published version of the manuscript.

Funding: This work has been supported by the National Natural Science Foundation of China (NSFC) (11304184), and the Shandong University of Technology and Zibo City Integration Development Project (2019ZBXC120). This work has been supported by the "Opening Foundation of Shandong Provincial Key Laboratory of Laser Technology and Application".

Data Availability Statement: Data underlying the results presented in this paper are not publicly available at this time but may be obtained from the authors upon reasonable request.

Conflicts of Interest: The authors declare that there are no conflicts of interest related to this article.

References

1. Zhang, Z.-X.; Mou, C.-B.; Yan, Z.-J.; Wang, Y.-J.; Zhou, K.-M.; Zhang, L. Switchable dual-wavelength Q-switched and mode-locked fiber lasers using a large-angle tilted fiber grating. *Opt. Express* **2015**, *23*, 1353–1360. [CrossRef] [PubMed]
2. Liu, X.-J.; Hong, Z.-F.; Liu, Y.; Zhang, H.-N.; Guo, L.-P.; Ge, X.-L. Few-layer TaSe2 as a saturable absorber for passively Q-switched erbium-doped fiber lasers. *Opt. Mater. Express* **2021**, *11*, 385–397. [CrossRef]
3. Hu, P.; Liu, F.-F.; Huang, Y.; Liu, Y.; Han, K.-Z.; Zhang, F.; Liu, X.-J. Passively Q-switched ytterbium-doped fiber laser operating at 1120 nm by molybdenum disulfide saturable absorber. *Optik* **2019**, *189*, 97–102. [CrossRef]
4. Hu, P.; Huang, Y.; Liu, F.-F.; Liu, Y.; Guo, L.-P.; Ge, X.-L.; Liu, X.-J. A Q-Switched Erbium-Doped Fiber Laser Based on ZrS_2 as a Saturable Absorber. *Chin. Opt. Lett.* **2019**, *17*, 080603. [CrossRef]
5. Luo, Z.-Q.; Zhou, M.; Weng, J.; Huang, G.-M.; Xu, H.-Y.; Ye, C.-C.; Cai, Z.-P. Graphene-based passively Q-switched dual-wavelength erbium-doped fiber laser. *Opt. Lett.* **2010**, *35*, 3709–3711. [CrossRef] [PubMed]
6. Khalid, U.S.; Asghar, H.; Hameed, H.; Sohail, M.; Khalil, A.; Ahmed, R.; Umar, Z.A.; Iqbal, J.; Baig, M.A. Q-switched pulse operation in erbium-doped fiber laser subject to zirconia (ZrO_2) nanoparticles-based saturable absorber. *Heliyon* **2024**, *10*, e24478. [CrossRef] [PubMed]
7. Liu, M.-L.; Liu, W.-J.; Yan, P.-G.; Fang, S.-B.; Teng, H.; Wei, Z.-Y. High-power $MoTe_2$-based passively Q-switched erbium-doped fiber laser. *Chin. Opt. Lett.* **2018**, *16*, 020007. [CrossRef]
8. Chernysheva, M.; Rozhin, A.; Fedotov, Y.; Mou, C.; Arif, R.; Kobtsev, S.M.; Dianov, E.M.; Turitsyn, S.K. Carbon nanotubes for ultrafast fibre lasers. *Nanophotonics* **2017**, *6*, 1–30. [CrossRef]
9. De Conti, M.C.M.D.; De Castro, A.A.; Assis, L.C.; Silva, R.A.; Silva, M.R.; Santos, M.J.; Silva, J.R.; La Porta, F.A.L. Carbon dots in the center of the spotlight: A full evaluation of their synthesis and understanding of their fundamental properties and applications. *Mater. Today Sustain.* **2024**, *27*, 100937. [CrossRef]
10. Pourmadadi, M.; Rahmani, E.; Rajabzadeh-Khosroshahi, M.; Samadi, A.; Behzadmehr, R.; Rahdar, A.; Ferreira, L.F.R. Properties and application of carbon quantum dots (CQDs) in biosensors for disease detection: A comprehensive review. *J. Drug Deliv. Sci. Technol.* **2023**, *80*, 104156. [CrossRef]
11. Devi, P.; Saini, S.; Kim, K.-H. The advanced role of carbon quantum dots in nanomedical applications. *Biosens. Bioelectron.* **2019**, *141*, 111158. [CrossRef] [PubMed]
12. Wang, R.; Lu, K.-Q.; Tang, Z.-R.; Xu, Y.-J. Recent progress in carbon quantum dots: Synthesis, properties and applications in photocatalysis. *J. Mater. Chem. A* **2017**, *5*, 3717–3734. [CrossRef]
13. Das, S.; Mondal, S.; Ghosh, D. Carbon quantum dots in bioimaging and biomedicines. *Front. Bioeng. Biotechnol.* **2024**, *11*, 1333752. [CrossRef] [PubMed]

14. Kong, J.-C.; Wei, Y.-H.; Zhou, F.; Shi, L.-T.; Zhao, S.-J.; Wan, M.-Y.; Zhang, X.-F. Carbon quantum dots: Properties, preparation, and applications. *Molecules* **2024**, *29*, 2002. [CrossRef]
15. Wang, Y.-F.; Hu, A.-G. Carbon quantum dots: Synthesis, properties and applications. *J. Mater. Chem. C* **2014**, *2*, 6921–6939. [CrossRef]
16. Molaei, M.J. Carbon quantum dots and their biomedical and therapeutic applications: A review. *RSC Adv.* **2019**, *9*, 6460–6481. [CrossRef] [PubMed]
17. Liu, X.-J.; Jiang, X.-W.; Liu, T.-R.; Xu, Y.; Zhang, W.-F. Generation of conventional soliton and 20th harmonic mode-locking in an erbium-doped fiber laser modulated by carbon-quantum-dots saturable absorbers. *Opt. Express* **2024**, *32*, 47236–47247. [CrossRef]
18. Sun, Y.-P.; Zhou, B.; Lin, Y.; Wang, W.; Fernando, K.A.S.; Pathak, P.; Meziani, M.J.; Harruff, B.A.; Wang, X.; Wang, H.-F.; et al. Quantum-sized carbon dots for bright and colorful photoluminescence. *J. Am. Chem. Soc.* **2006**, *128*, 7756–7757. [CrossRef] [PubMed]
19. Cao, L.; Wang, X.; Meziani, M.J.; Lu, F.-S.; Wang, H.-F.; Luo, P.G.; Lin, Y.; Harruff, B.A.; Veca, L.M.; Murray, D.; et al. Carbon dots for multiphoton bioimaging. *J. Am. Chem. Soc.* **2007**, *129*, 11318–11319. [CrossRef] [PubMed]
20. Bourlinos, A.B.; Karakassides, M.A.; Kouloumpis, A.; Gournis, D.; Bakandritsos, A.; Papagiannouli, I.; Aloukos, P.; Couris, S.; Hola, K.; Zboril, R.; et al. Synthesis, characterization and non-linear optical response of organophilic carbon dots. *Carbon* **2013**, *61*, 640–643. [CrossRef]
21. Ni, Y.-Q.; Li, X.-Y.; Liang, W.-Q.; Zhang, S.-F.; Xu, X.-S.; Li, Z.-Y.; Li, L.; Shao, Y.-H.; Ruan, S.-C.; Zhang, W.-F. Transformation of random lasing to Fabry–Perot lasing: Observation of high temperature lasing from carbon dots. *Nanoscale* **2021**, *13*, 7566–7573. [CrossRef] [PubMed]
22. Shi, P.-G.; Song, Y.-M.; Tang, J.; Nie, Z.-F.; Chang, J.-W.; Chen, Q.-Y.; He, Y.-F.; Guo, T.-T.; Zhang, J.; Wang, H. Ultra-narrow bandwidth red-emission carbon quantum dots and their bio-imaging. *Phys. E Low-Dimens. Syst. Nanostruct.* **2022**, *142*, 115197. [CrossRef]
23. Yuan, F.-L.; Yuan, T.; Sui, L.-Z.; Wang, Z.-B.; Xi, Z.-F.; Li, Y.-C.; Li, X.-H.; Fan, L.-Z.; Tan, Z.-A.; Chen, A.-M.; et al. Engineering triangular carbon quantum dots with unprecedented narrow bandwidth emission for multicolored LEDs. *Nat. Commun.* **2018**, *9*, 2249. [CrossRef] [PubMed]
24. Hong, Z.-F.; Zhang, M.-X.; Jiang, X.-W.; Wu, J.-W.; Zhang, H.-N.; Liu, X.-J. Generation of soliton molecules in mode-locked erbium-doped fiber laser by InSb saturable absorber. *Infrared Phys. Technol.* **2023**, *129*, 104540. [CrossRef]
25. Liu, X.-J.; Hu, P.; Liu, Y.; Guo, L.-P.; Ge, X.-L.; Zhang, H.-N. Conventional solitons and bound-state solitons in an erbium-doped fiber laser mode-locked by $TiSe_2$-based saturable absorber. *Nanotechnology* **2020**, *31*, 365202. [CrossRef] [PubMed]
26. Liu, X.-J.; Wang, G.-M.; Zhu, M.-X.; Han, K.-Z.; Zhang, W.-F.; Zhang, H.-N. Traditional soliton erbium-doped fiber laser with InSe as saturable absorber. *Front. Inf. Technol. Electron. Eng.* **2021**, *22*, 325–333. [CrossRef]
27. Ye, S.-S.; Huang, H.-B.; Chen, S.-Y.; Tao, J.-Z.; Wen, Y.-X.; Gao, W.-Q. 2.8 μm passively Q-switched mode-locked fiber laser using TiCN as saturable absorber. *Opto-Electron Eng.* **2023**, *50*, 230107. [CrossRef]
28. Yao, J.-N.; Jiang, X.-H.; Wang, A.-T.; Wang, J.-H.; Chen, R.-S.; Zhang, J.-L.; Zhan, Q.-W. Wavelength switchable Q-switched fiber laser based on Fe_3O_4 nanoparticles. *Optik* **2021**, *243*, 167279. [CrossRef]
29. Guo, G.-W.; He, W.; Chen, X.-Y.; Yang, S.-Y.; Li, Z.-H.; Ren, G.-H. Q-switched erbium-doped fiber laser based on SWNT saturable absorber combined with Sagnac filter. *Semicond. Optoelectron.* **2023**, *44*, 532–537. [CrossRef]
30. Ahmad, H.; Reduan, S.A.; Ruslan, N.E.; Lee, C.S.J.; Zulkifli, M.Z.; Thambiratnam, K. Tunable Q-switched erbium-doped fiber laser in the C-band region using nanoparticles (TiO_2). *Opt. Commun.* **2019**, *435*, 283–288. [CrossRef]
31. Muhammad, F.D.; Zulkifli, M.Z.; Ahmad, H. 1500-nm Q-switched fibre laser with carbon nanotubes. *Quantum Electron.* **2018**, *48*, 941–944. [CrossRef]
32. Shang, X.-X.; Xu, N.-N.; Zong, M.-Y.; Su, L.-Z.; Yu, W.-Y.; Guo, L.-G.; Gao, G.-G.; Zhang, Z.-Q.; Wang, Z.-H.; Zhang, H.-N. Nonlinear optical properties of $ZrGeTe_4$ at 1.5 μm for the passively Q-switched fiber laser. *J. Nonlinear Opt. Phys. Mater.* **2026**, 2650043. [CrossRef]
33. Dai, C.-S.; Dong, Z.-P.; Lin, J.-Q.; Yao, P.-J.; Xu, L.-X.; Gu, C. Passively Q-switched and mode-locked 1.9 μm Tm-doped fiber laser based on pure water as saturable absorber. *Acta Phys. Sin.* **2022**, *71*, 174202. [CrossRef]
34. Shang, X.-X.; Xu, N.-N.; Zong, M.-Y.; Yu, W.-Y.; Guo, L.-G.; Gao, G.-G.; Zhang, Z.-Q.; Zhang, H.-N.; Su, L.-Z. $ZrGeTe_4$ Nanoparticles as a Saturable Absorber for Mode-Locked Operations at 1 and 1.55 μm. *Photonics* **2026**, *13*, 305. [CrossRef]
35. Xu, N.-N.; Zong, M.-Y.; Su, L.-Z.; Wang, Z.; Yu, W.-Y.; Fan, W.-Y.; Guo, L.-G.; Fu, S.; Shang, X.-X.; Zhang, H.-N. Nonlinear optical properties of tellurene nanosheets for harmonic soliton operations in an Er-doped fiber laser. *Photonics* **2026**, *13*, 584. [CrossRef]
36. Yan, P.-G.; Liu, A.-J.; Chen, Y.-S.; Chen, H.; Ruan, S.-C.; Guo, C.-Y.; Chen, S.-F.; Li, I.L.; Yang, H.-P.; Hu, J.-G.; et al. Microfiber-based WS_2-film saturable absorber for ultra-fast photonics. *Opt. Mater. Express* **2015**, *5*, 479–489. [CrossRef]
37. Hou, S.-D.; Lu, C.-J.; Lin, H.-F.; Wang, J.-Z.; Guo, C.-Y.; Cheng, J.-Q.; Zhang, M.; Yan, P.-G. Ultrafast thulium-doped fiber laser mode-locked by antimonides. *Opt. Express* **2021**, *29*, 13722–13732. [CrossRef] [PubMed]

38. Cui, H.; Zhang, H.-C.; Ding, C.; Ding, Y.-Q.; Ju, Y.; Ma, X.-Q.; Lu, D.-Y.; Yun, L.; Yu, K.-H.; Wei, W. Stretched-pulse fiber laser mode-locked by PbS quantum dots. *Opt. Laser Technol.* **2022**, *151*, 107991. [CrossRef]
39. Ming, N.; Tao, S.-N.; Yang, W.-Q.; Chen, Q.-Y.; Sun, R.-Y.; Wang, C.; Wang, S.-Y.; Man, B.-Y.; Zhang, H.-N. Mode-locked Er-doped fiber laser based on PbS/CdS core/shell quantum dots as saturable absorber. *Opt. Express* **2018**, *26*, 9017–9026. [CrossRef] [PubMed]
40. Bogusławski, J.; Sotor, J.; Sobon, G.; Tarka, J.; Jagiello, J.; Macherzynski, W.; Lipinska, L.; Abramski, K.M. Mode-locked Er-doped fiber laser based on liquid phase exfoliated Sb_2Te_3 topological insulator. *Laser Phys.* **2014**, *24*, 105111. [CrossRef]
41. Liu, H.; Zheng, X.-W.; Liu, M.; Zhao, N.; Luo, A.-P.; Luo, Z.-C.; Xu, W.-C.; Zhang, H.; Zhao, C.-J.; Wen, S.-C. Femtosecond pulse generation from a topological insulator mode-locked fiber laser. *Opt. Express* **2014**, *22*, 6868–6873. [CrossRef] [PubMed]
42. Zhang, Y.-N.; Wu, K.-X.; Miao, T.; Xue, J.; Yao, Y.-M. Erbium-doped fiber laser based on copper oxide saturable absorber. *J. Appl. Opt.* **2023**, *44*, 684–692. [CrossRef]

Disclaimer/Publisher's Note: The statements, opinions and data contained in all publications are solely those of the individual author(s) and contributor(s) and not of MDPI and/or the editor(s). MDPI and/or the editor(s) disclaim responsibility for any injury to people or property resulting from any ideas, methods, instructions or products referred to in the content.